Performance Analysis of an UAV-assisted NOMA-based on MEC in IoT Network with Wireless Power Transfer

Gia-Huy Nguyen, Anh-Nhat Nguyen, Tung-Son Ngo, Ngoc-Anh Bui, Phuong-Chi Le, Manh-Duc Hoang, Tien-Dat Trinh, Khai Nguyen, and Minh-Sang Nguyen

ICT Department, FPT University, Hanoi 10000, Vietnam
{huynghe180064, khainhe176049, sangnmhe176048}@fpt.edu.vn
{nhatna3, sonnt69, anhbn5, chilp2, duchm29, datt67}@fe.edu.vn

Abstract. This article investigates an unmanned aerial vehicle (UAV)-assisted uplink non-orthogonal multiple access (NOMA) based on mobile-edge computing (MEC) with wireless power transfer (WPT) in Internet of Things (IoT) networks. Consider an urban scenario where an UAV embedded with a MEC sever helps two clusters of resource-restricted IoT devices (IDs) in providing energy and handling computational tasks. Accordingly, we propose a four-phased protocol called time switching (TS) - radio frequency (RF)-WPT UAV NOMA MEC (TS-RUNM), which comprises of harvesting energy, offloading tasks, computing data, and returning results. To assess the system performance, we derive the closed-form expressions of outage probability (OP) and successful computation probability (SCP) for the whole system in consideration of imperfect channel state information (ICSI) over Nakagami-m fading channel. Furthermore, we formulate system performance optimization problems with the goal of minimizing OP and maximizing SCP. The solution is based on particle swarm optimization (PSO) algorithm that establishes optimal values for UAV's position and altitude. In addition, the Monte Carlo simulations are conducted with diverse system parameters to validate the precision of our study.

Keywords: internet of things, unmanned aerial vehicles, wireless power transfer, non-orthogonal multiple access, mobile edge computing, particle swarm optimization, imperfect channel state information

1 Introduction

With the exponential growth of Internet of Things (IoT) devices, the pressing requirement for robust and sustainable wireless communication links is deemed to be vital [1–3]. Nevertheless, traditional IoT network infrastructure remains static with substantial deployment costs and restricted transmission coverage. Moreover, the presence of large buildings or dense foliage can pose significant signal blockage, leading to the reduction of data throughput [4].

Unmanned aerial vehicle (UAV) has emerged as a feasible solution in response to these deficiencies. Due to its inherent advantages including exceptional mobility and minimal operating costs, UAV is consequently utilized in transmitting data between the sever and multiple IoT devices (IDs), as demonstrated in [5]. One critical advantage of UAV is the ability to establish the Line-of-Sight (LoS) connections with IDs, fostering several benefits such as signal coverage enhancements, avoidance of large-scale fading that can hinder communication links, and overall network performance robustness [6]. For example, Bithas *et al.* [7] introduced an UAV selection policy considering the effect of LoS, Non-LoS (NLoS), and mobility to exploit the best received signals. In addition, another posed issue for IDs and UAV is power-constrained.

Hence, the deployment of wireless power transfer (WPT) has been presented as a compelling solution for the IoT network [8]. The author in [9] proposed that the applications of WPT-enabled radio frequency (RF) in wireless communication offers a long-term and consistent power source for mobile devices compared to natural sources, which are contingent on the stochastic environment conditions. Furthermore, due to IDs' small size and short-capacity batteries, they are unable to process intensive workloads independently.

In order to counteract this challenge, mobile-edge computing (MEC) emerges as a possible approach in IoT networks [10]. Power-limited devices can offload a portion or entire computational tasks to MEC severs positioned in the proximity of the network edge for data calculation. This helps IoT networks to tremendously reduce the overall latency, minimize the power depletion, and enhance the quality of communication links [11]. Furthermore, non-orthogonal multiple access (NOMA) permits a large number of mobile devices to simultaneously access IoT network and radio resources by exploiting multiple power domains [12]. In other terms, NOMA has the advantages of transmitting an extraordinarily large amount of data and enhancing spectral efficiency.

Driven by the preceding discourses, this paper studies an UAV-assisted uplink NOMA based on MEC with WPT over Nakagami-m fading channel for IoT networks. We consider that IDs harvest RF broadcast energy from UAV for offloading tasks. Additionally, we evaluate the probability of LoS and NLoS between UAV and IDs wireless communication. Finally, we propose an optimization problem to enhance the performance of the system. The following are the primary contribution of our paper:

- We studied an UAV-assisted NOMA MEC with WPT over Nakagami-m distribution in IoT networks. In addition, we considered the imperfect channel state information (ICSI) associated with the best ID selection (BIS) scheme. Accordingly, we proposed a communication protocol for effective energy harvesting and offloading tasks, called time switching (TS) - RF-WPT UAV NOMA MEC (TS-RUNM).
- We derived closed-form expressions of outage probability (OP) and successful computation probability (SCP) for the whole system. Moreover, we formulated a problem to minimize OP and maximize SCP by optimizing the UAV's position and altitude. The problem was solved based on PSO algorithm.

– Numerical results were presented to verify the system performance using diverse parameters including UAV's transmit power, the number of IDs in two clusters, the channel estimation error variance, UAV's position and altitude.

The paper's remaining section is organized as follows. In Section 2, the system model and communication protocol are demonstrated. The OP, SCP, and optimization problem are examined in Section 3. Section 4 discusses the numerical results. The final conclusions are summarized in Section 5.

2 System Model and Communication Protocol

2.1 System and Channel Model

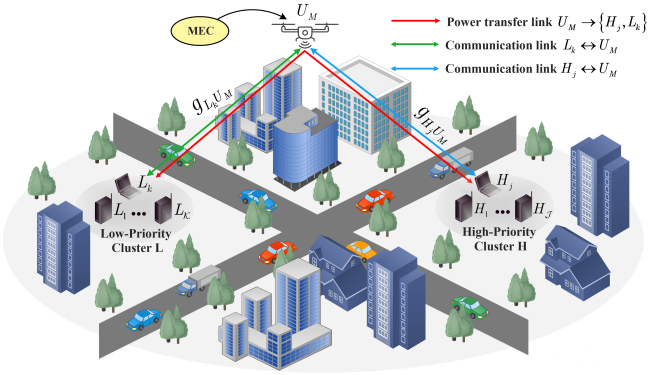

Fig. 1: System model for the RUNM in IoT networks.

As demonstrated in Fig. 1, we consider a system model in the IoT networks, including an UAV-assisted uplink NOMA based on MEC with RF-WPT, denoted by U_M, high-priority cluster H comprising $\mathcal{J}$ devices, denoted by H_j, $j \in (1, ..., \mathcal{J})$, and low-priority cluster L comprising $\mathcal{K}$ devices, denoted by L_k, $k \in (1, ..., \mathcal{K})$. Due to power-constraints and the incapacity to carry out complex computations, IDs in two clusters initially harvest RF broadcast energy from U_M before offloading their tasks to the MEC sever for data handling. We assume that all devices within the system are equipped with a single antenna operating in a half-duplex mode and in an urban scenario. Furthermore, it is posited that the IDs execute identical tasks of length l (bits) and are independently categorized into discrete groups [13]. Therefore, the offloaded capacity of both clusters is expressed as $\mathcal{C}_i^{off} = \beta_i l$, where β_i, $i \in (j, k)$, $(0 \leq \beta_i \leq 1)$, is the offloading ratio.

To model spatial relationships of the system components, we adopt a 3D Cartesian coordinate system, in which the UAV is positioned at U_M (x_U, y_U, h_U), while the ID clusters are situated at ground level with coordinates H_j $(x_j, y_j, 0)$

and $L_k\left(x_k, y_k, 0\right)$. Supposing the large-scale fading channel between UAV and devices is characterized by the LoS and NLoS probabilistic model. By incorporating the respective probabilities of LoS and NLoS conditions, the mean path loss is expressed as follows [13]:

$$\overline{\mathcal{L}}_{ab} = \left[\frac{\mathbb{V}^{los} - \mathbb{V}^{nlos}}{1 \; + \; \mu_1 e^{-\mu_2(\theta_{ab}-\mu_1)}} + \mathbb{V}^{nlos}\right] \mathcal{D}_{ab}^{\sigma}, \tag{1}$$

where $ab \in (H_j U_M, L_k U_M)$, $\mathbb{V}^{los} = \xi^{los}\left(\frac{c}{4\pi f_c}\right)^{-1}$, $\mathbb{V}^{nlos} = \xi^{nlos}\left(\frac{c}{4\pi f_c}\right)^{-1}$, μ_1 and μ_2 are the environment values; $\theta_{ab} = \frac{180}{\pi}\arcsin(\frac{h_U}{\mathcal{D}_{ab}})$ is the elevation angle; $\mathcal{D}_{ab} = \sqrt{\left(x_b - x_a\right)^2 + \left(y_b - y_a\right)^2 + h_U^2}$ is the distance from a to b; σ is the path loss exponent; ξ^{los} and ξ^{nlos} are excessive path losses of LoS and NLoS communication between U_M and IDs; c and f_c are the speed of light and the carrier frequency, respectively.

We assume the channel coefficients are independent and follow Nakagami-m distribution which is modeled by using the minimum mean square error channel estimation error as in [12]. Hence, the channel coefficient considering imperfect channel state information (ICSI) can be written as $g_{ab} = \tilde{g}_{ab} + \Omega_{ab}$,where $\tilde{g}_{ab}$ is the estimated channel coefficient, Ω_{ab} is the channel estimation error approximated by the Gaussian random variable distribution, $\Omega_{ab} \sim \mathcal{CN}\left(0, \varepsilon_{ab}\right)$. Within this paper, we consider the variance of the channel estimation error ε_{ab} is constant [14].

By estimating the maximum signal-to-noise ratios (SNRs) of $U_M - H_j$ and $U_M - L_k$ links, an optimal offloading ID selection strategy is implemented. Accordingly, the best channel gain for the BISs in two clusters is achieved by: $|\tilde{g}_{i^*}|^2 = \max\left\{|\tilde{g}_{I_{i^*}U_M}|^2\right\}$, where $i^* \in (j^*, k^*)$, $I \in (H, L)$. The system model is posited to be affected by Nakagami-m distribution, so the cumulative distribution function (CDF) and probability density function (PDF) of the channel power gains $|\tilde{g}_{i^*}|^2$ are expressed as:

$$F_{|\tilde{g}_{i^*}|^2}\left(x\right) = \sum_{z=0}^{\mathcal{Z}} \Phi_z (-1)^z \Xi_{1,z} \Xi_{2,z} x^{\bar{z}} e^{-\frac{zxm}{\lambda_{ab}}}, \tag{2}$$

$$f_{|\tilde{g}_{i^*}|^2}\left(x\right) = \frac{\mathcal{Z} x^{m-1}}{(m-1)!}\left(\frac{m}{\lambda_{ab}}\right)^m e^{-\frac{xm}{\lambda_{ab}}} \sum_{z=0}^{\mathcal{Z}-1} \Phi_z (-1)^z \Xi_{1,z} \Xi_{2,z} x^{\bar{z}} e^{-\frac{zxm}{\lambda_{ab}}}, \tag{3}$$

where $\mathcal{Z} = \{\mathcal{J}, \mathcal{K}\}$, $z = \{t, h, p\}$, $\Phi_z = \sum\limits_{z_1=0}^{z} \sum\limits_{z_2=0}^{z-z_1} ... \sum\limits_{z_{m-1}=0}^{z-z_1-z_2-...-z_{m-2}}$, $\Xi_{1,z} = \binom{\mathcal{Z}}{z}\binom{z}{z_1}\binom{z-z_1}{z_2}...\binom{z-z_1-z_2-...-z_{m-2}}{z_{m-1}}$, $\Xi_{2,z} = \prod\limits_{s=0}^{m-2}\left[\frac{1}{s!}\left(\frac{m}{\lambda_{ab}}\right)^s\right]^{z_{s+1}} \times \left[\frac{1}{(m-1)!}\left(\frac{m}{\lambda_{ab}}\right)^{m-1}\right]^{z-z_1-z_2...-z_{m-1}}$, $\bar{z} = (m-1)(z-z_1) - (m-2)z_2 - ... - z_{m-1}$, $m \in (2, 3, 4, ...)$.

2.2 Communication Protocol

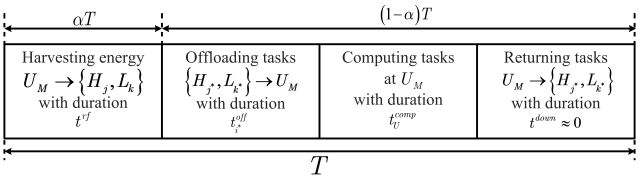

Fig. 2: TS-RUNM communication protocol.

This subsection discusses the TS-RUNM protocol for the proposed system. Depicted in Fig. 2, the protocol is described as follows:

- In the first phase t^{rf}: U_M transmits RF broadcast power to the two ID clusters for energy harvesting. Thereafter, the two BISs, designated as H_{j^*} and L_{k^*}, are selected based on the highest SNRs from their respective clusters. Thus, the transmitted energy to the IDs can be expressed as $E_{i^*} = \frac{\eta P_U \alpha T |g_{i^*}|^2}{\overline{\mathcal{L}}_{i^*}}$, where η, $(0 < \eta < 1)$, is the energy harvesting efficiency coefficient; P_U is power transmission of U_M; α is the TS ratio, $(0 < \alpha < 1)$; T is transmission block time.
- During the second phase $t_{i^*}^{off}$: The two BISs from two clusters concurrently offload their tasks via uplink NOMA resulting in the composite signal obtained at U_M:

$$y_U^M = \sqrt{\frac{P_{j^*}}{\overline{\mathcal{L}}_{j^*}}} \left(\tilde{g}_{j^*} + \Omega_{j^*}\right) x_{j^*} + \sqrt{\frac{P_{k^*}}{\overline{\mathcal{L}}_{k^*}}} \left(\tilde{g}_{k^*} + \Omega_{k^*}\right) x_{k^*} + n_U, \tag{4}$$

where $P_{i^*} = \frac{E_{i^*}}{(1-\alpha)T - t_U^{comp}}$ is the power transmit of the BIS to UAV; x_{j^*} and x_{k^*} are the signal of H_{j^*} and L_{k^*}; $n_U \sim \mathcal{CN}(0, \mathcal{N}_0)$ is distributed by the additive white Gaussian noise (AWGN). Here, U_M commences the signal decoding processes of x_{j^*} and x_{k^*} by employing successive interference cancellation (SIC) [12]. Hence, this process results in the following expressions of the signal-to-interference-plus-noise ratios (SINRs) for x_{j^*} and x_{k^*}:

$$\gamma_{j^*}^U = \frac{z_1 x^2}{z_2 y^2 + z_3}, \tag{5}$$

$$\gamma_{k^*}^U = \frac{z_2 y^2}{z_4}, \tag{6}$$

where $z_1 = \frac{\gamma_{j^*}}{\overline{\mathcal{L}}_{j^*}}$, $z_2 = \frac{\gamma_{k^*}}{\overline{\mathcal{L}}_{k^*}}$, $z_3 = z_1 \varepsilon_{j^*}^2 + z_2 \varepsilon_{k^*}^2 + 1$, $z_4 = z_2 \varepsilon_{k^*}^2 + 1$, $\gamma_{j^*} = \frac{\eta \gamma_U \alpha T}{\overline{\mathcal{L}}_{j^*}[(1-\alpha)T - t_U^{comp}]}$, $\gamma_{k^*} = \frac{\eta \gamma_U \alpha T}{\overline{\mathcal{L}}_{k^*}[(1-\alpha)T - t_U^{comp}]}$, $\gamma_U = \frac{P_U}{\mathcal{N}_0}$.

– During the third phase t_U^{comp}: The offloaded tasks undergo calculation at MEC sever. The temporal duration necessary for the completion of these computational processes with a number of task bits is expressed as follows $t_U^{comp} = \frac{(\mathcal{C}_{j^*}^{off}+\mathcal{C}_{k^*}^{off})\varpi}{f_U^M}$, where ϖ is the number of CPU cycles requires to compute a single task bit and f_U^M is the MEC's operating frequency at U_M.
– In the final phase t^{down}: The computed results are returned to the BIS that correspond to its cluster. Since retrieving data requires minor power and brief time-latency, t^{down} can consequently be ignored [15].

3 Performance Analysis

3.1 Outage Probability (OP)

This subsection focuses on deriving an analytical expression for the OP of the proposed RUNM system, denoted by OPs, defined as the likelihood that the instantaneous channel capacity C_{i^*} encounters an outage event and drops below a predetermined rate $R_{i^*}^{th}$. Hence, the OPs for the whole system is expressed as:

$$OPs = \Pr\left\{C_{j^*} < R_{j^*}^{th} \cup C_{k^*} < R_{k^*}^{th}\right\} = 1 - \Pr\left\{C_{j^*} > R_{j^*}^{th}, C_{k^*} > R_{k^*}^{th}\right\}, \quad (7)$$

where $C_{i^*} = WT^{th}\log_2\left(1+\gamma_{i^*}^U\right)$; W is the bandwidth; $T^{th} = (1-\alpha)T - t_U^{comp}$.

Lemma 1. *The closed-form expression for the OP of the whole RUNM system across Nakagami-m fading channel is formulated as follows:*

$$OPs = F\left(\Theta_c\right) + \frac{\pi e^{-\Theta_c}\mathcal{K}}{2Q\left(m-1\right)!}\left(\frac{m}{\lambda_{UB}}\right)^m \sum_{h=0}^{\mathcal{J}} \Phi_h(-1)^h \Xi_{1,h}\Xi_{2,h} \sum_{p=0}^{\mathcal{K}-1} \Phi_p(-1)^p \Xi_{1,p}$$
$$\times\, \Xi_{2,p} \sum_{q=1}^{Q} \sqrt{1-\varphi_q^2}\left(\Theta^{(\Psi_q)}\right)^{\bar{h}} \Psi_q^{m+\bar{p}-1} e^{-\frac{hm}{\lambda_{UA}}\Theta^{(\Psi_q)}} \omega_q^{\frac{m(p+1)}{\lambda_{UB}}-1}, \quad (8)$$

where $F\left(\Theta_c\right) = \sum_{t=0}^{\mathcal{K}} \Phi_t(-1)^t \Xi_{1,t}\Xi_{2,t}(\Theta_c)^{\bar{t}} e^{-\frac{tm}{\lambda_{UB}}\Theta_c}$, $\Theta_c = \sqrt{\frac{\gamma_{k^*}^{th} z_4}{z_2}}$, $\gamma_{k^*}^{th} = 2^{\frac{R_{k^*}^{th}}{WT^{th}}} - 1$, $\varphi_q = \cos\left(\frac{\pi(2q-1)}{2Q}\right)$, $\Theta^{(\Psi_q)} = \sqrt{\frac{\gamma_{j^*}^{th}\left(z_2\Psi_q^2+z_3\right)}{z_1}}$, $\Psi_q = -\ln(\omega_q)$, $\omega_q = \frac{(\varphi_q+1)e^{-\Theta_c}}{2}$, $\gamma_{j^*}^{th} = 2^{\frac{R_{j^*}^{th}}{WT^{th}}} - 1$, *and* Q *is the complexity-vs-accuracy trade-off coefficient* [16].

Proof. See Appendix A.

3.2 Successful Computation Probability (SCP)

This subsection focuses on deriving the mathematical expression for the SCP of the RUNM system, denoted as $SCPs$, calculated as the possibility that all duration of the offloaded tasks accomplishes within the prescribed latency threshold T^{th}. Thus, the $SCPs$ for the whole system is given as:

$$SCPs = \Pr\left\{\max\left(t_{j^*}^{off}, t_{k^*}^{off}\right) < T^{th}\right\} = \Pr\left\{t_{j^*}^{off} < T^{th}, t_{k^*}^{off} < T^{th}\right\}, \quad (9)$$

where $t_{i^*}^{off} = \frac{\mathcal{C}_{i^*}^{off}}{WT^{th}\log_2\left(1+\gamma_{i^*}^{U}\right)}$.

Lemma 2. *The closed-form expression for the SCP of the whole RUNM system across Nakagami-m fading channel is expressed as:*

$$SCPs = 1 - F\left(\Delta_c\right) - \frac{\pi e^{-\Delta_c}\mathcal{K}}{2Q\left(m-1\right)!}\left(\frac{m}{\lambda_{UB}}\right)^m \sum_{h=0}^{\mathcal{J}} \Phi_h(-1)^h \Xi_{1,h}\Xi_{2,h} \sum_{p=0}^{\mathcal{K}-1} \Phi_p(-1)^p$$
$$\times\, \Xi_{1,p}\Xi_{2,p} \sum_{l=1}^{Q} \sqrt{1-\varphi_l^2}\left(\Delta^{(\Psi_l)}\right)^{\bar{h}} \Psi_l^{m+\bar{p}-1} e^{-\frac{hm}{\lambda_{UA}}\Delta^{(\Psi_l)}} \omega_l^{\frac{m(p+1)}{\lambda_{UB}}-1}, \tag{10}$$

where $F\left(\Delta_c\right) = \sum_{t=0}^{\mathcal{K}} \Phi_t(-1)^t \Xi_{1,t}\Xi_{2,t}(\Delta_c)^{\bar{t}} e^{-\frac{tm}{\lambda_{UB}}\Delta_c}$, $\Delta_c = \sqrt{\frac{\delta_K z_4}{z_2}}$, $\delta_K = 2^{\frac{\mathcal{C}_{k^*}^{off}}{W(T^{th})^2}} - 1$, $\varphi_l = \cos\left(\frac{\pi(2l-1)}{2Q}\right)$, $\Delta^{(\Psi_l)} = \sqrt{\frac{\delta_J\left(z_2\Psi_l^2+z_3\right)}{z_1}}$, $\Psi_l = -\ln(\omega_l)$, $\omega_l = \frac{(\varphi_l+1)e^{-\Delta_c}}{2}$, $\delta_J = 2^{\frac{\mathcal{C}_{j^*}^{off}}{W(T^{th})^2}} - 1$.

Proof. See Appendix B.

3.3 System Performance Optimization: Problems and Solution

This subsection introduces a PSO-based solution for minimizing the OP, while considering SCP maximization situation of the whole system by determining the most optimal position and altitude of UAV, designated as (x_U^*, y_U^*, h_U^*). The optimization problems are formulated as follows:

– The OP minimization, denoted by (P1):

$$\begin{aligned}
\text{(P1):}\ \underset{x_U, y_U, h_U}{\text{minimize}} \quad & OPs \\
\text{subject to} \quad & 0 \le x_U \le x_U^{\max}, && \text{(11a)} \\
& 0 \le y_U \le y_U^{\max}, && \text{(11b)} \\
& 0 \le h_U \le h_U^{\max}. && \text{(11c)}
\end{aligned}$$

– The SCP maximization, denoted by (P2):

$$\begin{aligned}
\text{(P2):}\ \underset{x_U, y_U, h_U}{\text{maximize}} \quad & SCPs \\
\text{subject to} \quad & 0 \le x_U \le x_U^{\max}, && \text{(12a)} \\
& 0 \le y_U \le y_U^{\max}, && \text{(12b)} \\
& 0 \le h_U \le h_U^{\max}, && \text{(12c)}
\end{aligned}$$

where (11), (12) constraints are the conditions of UAV's position and altitude. To address the UAV's constraints and achieve optimal outcomes, we have utilized

PSO algorithm [13] with distinct fitness functions, each tailored to a specific optimization problem. Accordingly, **Algorithm 1** is applied to cope with the challenge in (P1) and (P2). The algorithm commences by selecting N iterations and O swarm particles with unique particle positions $\mathcal{X}_o\,(x_U, y_U, h_U)$ and velocity $\mathcal{V}_o$ according to problem constraints. Every particle generates a distinct objective function value based on its positions, and preserves a memory of its most fruitful position, called the personal best $\mathcal{P}_o$. Particle with the highest personal best position becomes the social best position $\mathcal{S}_o$ of the whole swarm. The position, the velocity, the personal best position, and the social best position are updated for every iteration. After the termination of PSO algorithm, the final social best position is returned.

Algorithm 1 PSO OPMin-SCPMax

Set initial values for PSO parameters: r, ∂_1, ∂_2, N, O;
Randomly select values between $[0, 1]$: τ_1, τ_2;
for $n = 1$ to N do **do**
  for $o = 1$ to O do **do**
    Randomly initialize the position: $\mathcal{X}_o$;
    Set the velocity: $\mathcal{V}_o = 0$;
    Set the personal and social best positions: $\mathcal{P}_o$, $\mathcal{S}_o$;
    Update new position: $\mathcal{X}_o^{n+1} = \mathcal{X}_o^n + \mathcal{V}_o^{n+1}$;
    Update new velocity: $\mathcal{V}_o^{n+1} = r\mathcal{V}_o^n + \partial_1\tau_1\,(\mathcal{P}_o^n - \mathcal{X}_o^n) + \partial_2\tau_2\,(\mathcal{S}_o^n - \mathcal{X}_o^n)$;
    Fitness functions for the corresponding case:
      $\mathcal{F} = OPs\,(\mathcal{X}_o)$, used when optimizing OP
      $\mathcal{F} = 1 - SCPs\,(\mathcal{X}_o)$, used when optimizing SCP
    Update the personal best position:
    if $\mathcal{F}\left(\mathcal{X}_o^{n+1}\right) \geq \mathcal{F}\,(\mathcal{P}_o^n)$ **then**
      $\mathcal{P}_o^{n+1} = \mathcal{X}_o^{n+1}$;
      if $\mathcal{F}\left(\mathcal{X}_o^{n+1}\right) < \mathcal{F}\,(\mathcal{P}_o^n)$ **then**
        $\mathcal{P}_o^{n+1} = \mathcal{P}_o^n$;
      end if
    end if
    Update the social best position: $\mathcal{S}_o^n = \max\,(\mathcal{P}_o^n)$;
    if $\mathcal{F}\,(\mathcal{X}_o^n) < \mathcal{F}\,(\mathcal{S}_o^n)$ **then**
      $\mathcal{S}_o^n = \mathcal{P}_o^n$;
    end if
  end for
end for
Return: $\mathcal{F}(\mathcal{S}_o^n)$ is the optimal value based on its respective fitness function.

Table 1: Parameters table

Parameters	Value	Parameters	Value	Parameters	Value
(x_j, y_j)	$(60, 60)$ (m)	ϖ	100	σ	2
(x_k, y_k)	$(20, 20)$ (m)	f_U^M	10^8 (Hz)	c	3.10^8
x_U	$(0, 60)$ (m)	μ_1	0.1581	f_c	3.10^6 (Hz)
y_U	$(0, 60)$ (m)	μ_2	9.6177	η	0.85
h_U	$(0, 300)$ (m)	ξ^{los}	1	α	$(0, 1)$
$\mathcal{C}_{j^*}^{off}$	$0.6.10^2$	ξ^{nlos}	20	T	1 (s)
$\mathcal{C}_{k^*}^{off}$	$0.4.10^2$	γ_U	$(0, 20)$ (dB)	W	8.10^8 (Hz)
$R_{j^*}^{th}$	400 (bit/s/Hz)	N	100	Q	10^3
$R_{k^*}^{th}$	400 (bit/s/Hz)	O	50	m	2

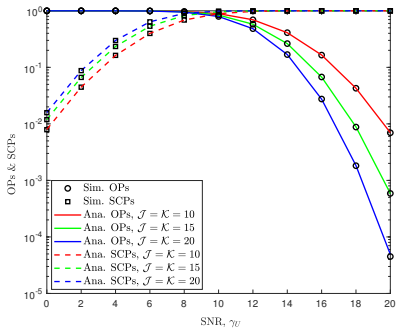

Fig. 3: Effect of the UAV's average transmit SNR γ_U on OP and SCP of the whole system with different number of IDs.

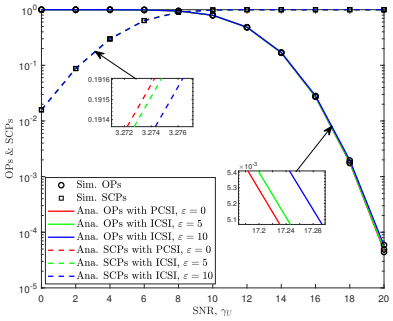

Fig. 4: Effect of perfect channel state information (PCSI) and ICSI on OP and SCP of the whole system.

4 Numerical Results

In this section, the numerical simulations are implemented to validate the mathematical expressions of the OP and SCP for the proposed system. The values for system parameters in all simulations is specified in the Table 1.

Fig. 3 depicts the effect of the UAV's average transmit power γ_U with different $\mathcal{J}$ and $\mathcal{K}$ IDs. The remarkable alignment between the Monte-Carlo simulations and our analytical results serves as a validation of the proposed model's exactness. Furthermore, the finding reveals that the simultaneous increase in the number of devices within both clusters demonstrably degrades OP while elevating SCP. This is due to the expanded pool of BIS candidates allowing UAV to select a better device. Additionally, a higher transmit SNR contributes to the degradation of OP and the augmentation of SCP, as IDs are provided more power to efficiently offload duties.

Fig. 4 demonstrates the effect of PCSI and ICSI on the proposed system. When the channel estimation error variance increases, both OP and SCP dis-

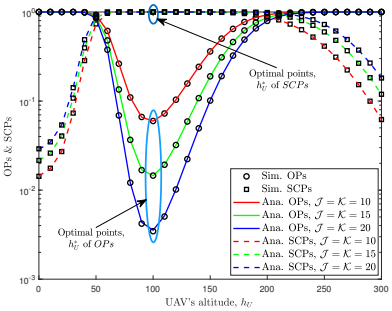

Fig. 5: Effect of the UAV's altitude h_U on OP and SCP of the whole system with different number of IDs.

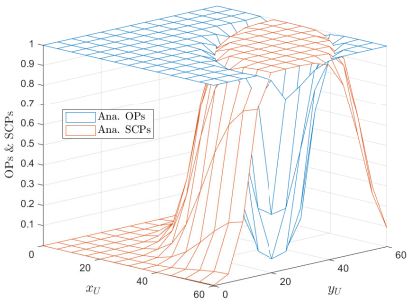

Fig. 6: Effect of the UAV's position (x_U, y_U) on OP and SCP of the whole system.

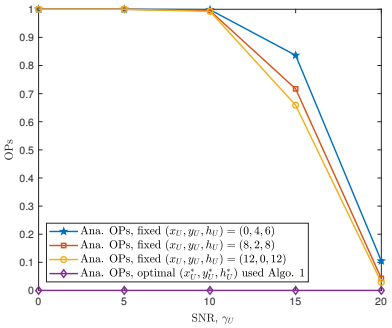

Fig. 7: Effect of the optimal $U(x_U^*, y_U^*, h_U^*)$ on OP of the whole system.

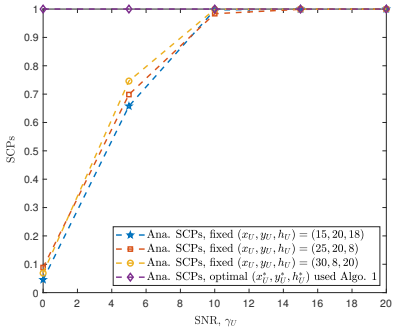

Fig. 8: Effect of the optimal $U(x_U^*, y_U^*, h_U^*)$ on SCP of the whole system.

play a prominent downward trend. This observation indicates that PCSI has a superior influence on the system performance compared to ICSI. However, acquiring PCSI in a dynamic channel environment is significantly challenging for the IDs due to hardware limitations and network connectivity issues.

The effect of the UAV's altitude on the OP and SCP outcomes is demonstrated in Fig. 5. We observe that there exists an ideal point of UAV's altitude h_U^* for which the OP is minimized, while the SCP is maximized. This can be explained by the characteristics of LoS and NLoS between UAV-IDs reception. When the altitude of the UAV is increased, the probability of encountering LoS becomes greater than the probability of NLoS. Nevertheless, the higher h_U results in the greater pass-loss and consequently decreases the system performance.

Apart from altitude optimization, determining the position of the UAV to strengthen transmission links is also crucial. Shown in Fig. 6, the 3D result

illustrates the OP and SCP value domains as influenced by the effect of x_U and y_U. We observe that there also exists an x_U^* and y_U^* position that minimizes OP and maximizes SCP. This observation aligns with the intuition that the UAV seeks a position that fosters the most favorable communication conditions.

Fig. 7 and Fig. 8 reveal the effect of the optimal position and altitude of UAV on OP and SCP of the whole system. We compare the optimal (x_U^*, y_U^*, h_U^*) of OP and SCP to fixed (x_U, y_U, h_U) values. The results demonstrate that by employing **Algorithm 1**, the OP value approaching zero indicates an exceptional system performance, while the SCP value is equal to one representing the system's maximal computational capability. In addition, the optimal values return the minimum OP value, and maximum SCP value compared to the self-fixed points.

5 Conclusion

In this paper, an UAV-assisted NOMA MEC with WPT in IoT networks over Nakagami-m fading channel was studied. We proposed a four-phased system protocol, called TS-RUNM, with the BIS selection scheme. For system performance assessment, we derived closed-form expressions of OP and SCP for the whole system. To optimize OP and SCP, we also proposed a PSO-based algorithm for determining the UAV's positions and altitude. Simulation results were presented to confirm the performance of the proposed system. In the future research direction, this proposed work will be extended to further fulfill the system performance such as obtaining the optimal TS ratio, exploring the case of multiple antenna. Furthermore, the conventional PSO algorithm optimization remains inefficient in the case of concurrently seeking optimal solutions for OP and SCPs. Hence, multi-objective optimizations could be employed for the future work.

A Proof of Lemma 1

By combining the expressions of (1), (5), (6) into (7), we can express the OPs of the system as:

$$OPs = 1 - \int_{\Theta_c}^{\infty} \int_{\Theta^{(y)}}^{\infty} f_x(x) f_y(y) dxdy = F_y(\Theta_c) + \underbrace{\int_{\Theta_c}^{\infty} F_x\left(\Theta^{(y)}\right) f_y(y) dy}_{I_1}, \quad (13)$$

where $\Theta_c = \sqrt{\frac{\gamma_{k^*}^{th} z_4}{z_2}}$, $\Theta^{(y)} = \sqrt{\frac{\gamma_{j^*}^{th}(z_2 y^2 + z_3)}{z_1}}$, $y = |\tilde{g}_{k^*}|^2$, $x = |\tilde{g}_{j^*}|^2$, $z_4 = z_2\varepsilon_{k^*}^2 + 1$, $z_2 = \frac{\gamma_{k^*}}{\overline{\mathcal{L}}_{k^*}}$, $z_3 = z_1\varepsilon_{j^*}^2 + z_2\varepsilon_{k^*}^2 + 1$, $z_1 = \frac{\gamma_{j^*}}{\overline{\mathcal{L}}_{j^*}}$, $\gamma_{j^*} = \frac{\eta\gamma_U \alpha T}{\overline{\mathcal{L}}_{j^*}[(1-\alpha)T - t_U^{comp}]}$, $\gamma_{k^*} = \frac{\eta\gamma_U \alpha T}{\overline{\mathcal{L}}_{k^*}[(1-\alpha)T - t_U^{comp}]}$, $\gamma_U = \frac{P_U}{\mathcal{N}_0}$. I_1 in (13) is sequentially solved by applying the CDF and PDF of the Nakagami-m distribution in (2), (3). Moreover, with the aid of the Gaussian-Chebyshev Quadrature in [16], the close-formed expression of OP is obtained as (8).

B Proof of Lemma 2

Similarly substituting as (13), we rewrite the $SCPs$ of (9) as follows:

$$SCPs = \int_{\Delta_c}^{\infty} \int_{\Delta^{(y)}}^{\infty} f_x(x) f_y(y) dx dy = \underbrace{\int_{\Delta_c}^{\infty} f_y(y) dy}_{I_2} - \underbrace{\int_{\Delta_c}^{\infty} F_x\left(\Delta^{(y)}\right) f_y(y) dy}_{I_3}, \quad (14)$$

where $\Delta_c = \sqrt{\frac{\delta_K z_4}{z_2}}$, $\Delta^{(y)} = \sqrt{\frac{\delta_J (z_2 y^2 + z_3)}{z_1}}$, $\delta_K = 2^{\frac{c_{k^*}^{off}}{W(T^{th})^2}} - 1$, $\delta_J = 2^{\frac{c_{j^*}^{off}}{W(T^{th})^2}} - 1$. I_2 and I_3 in (14) can be solved by applying the CDF and PDF of the Nakagami-m distribution in (2), (3). Moreover, with the aid of the Gaussian-Chebyshev Quadrature in [16], the close-formed expression of OP is obtained as (10).

References

1. A.-N. Nguyen, T.-S. Ngo, N.-A. Bui, P.-C. Le, and G.-H. Nguyen: UAV-aided uplink NOMA based on MEC in IoT networks: Secrecy offloading and Optimization. In: 7th SaSeIoT, pp. 131–146 (2024).
2. A.-N. Nguyen, D.-B. Ha, V. T. Truong, C. So-In, P. Aimtongkham, C. Sakunrasrisuay, and C. Punriboon: On Secrecy Analysis of UAV-Enabled Relaying NOMA Systems with RF Energy Harvesting. In: INISCOM, pp. 267–281 (2022).
3. L. R. Cenkeramaddi, A. Goyal, A. Bhuria, M. B. Srinivas, and J. Soumyai: Design of Software and Data Analytics for Self-Powered Wireless IoT Devices. In: iSES (2018).
4. Y. Guo, C. You, C. Yin, and R. Zhang: UAV Trajectory and Communication Co-Design: Flexible Path Discretization and Path Compression. In: IEEE J. on Sel. Areas., vol. 39, no. 11, pp. 3506–3523 (2021).
5. N. Abbas, A. Mrad, A. Ghazleh, and S. Sharafeddine: UAV-Based Relay System for IoT Networks With Strict Reliability and Latency Requirements. In: IEEE Net. Let., vol. 3, no. 3, pp. 110–113 (2021).
6. A.-N. Nguyen, D.-B. Ha, V.-N. Vo, V.-T. Truong, D.-T. Do, and C. So-In: Performance Analysis and Optimization for IoT Mobile Edge Computing Networks With RF Energy Harvesting and UAV Relaying. In: IEEE Access, (2022).
7. P. S. Bithas, V. Nikolaidis, A. G. Kanatas, and G. K. Karagiannidis: UAV-to-Ground Communications: Channel Modeling and UAV Selection. In: IEEE Trans. on Comm., vol. 68, no. 8, pp. 5135–5144 (2020).
8. Z. Zhang, H. Pang, A. Georgiadis, and C. Cecati: Wireless Power Transfer—An Overview. In: IEEE Trans. on Indus. Elec., vol. 66, no. 22, pp. 1044–1058 (2019).
9. T. D. P. Perera, D. N. K. Jayakody, S. K. Sharma, S. Chatzinotas, and J. Lii: Simultaneous Wireless Information and Power Transfer (SWIPT): Recent Advances and Future Challenges. In: IEEE Comm. Sur. & Tutor., no. 1, pp. 264–302 (2018).
10. A.-N. Nguyen and N.-A. Bui: Performance Analysis of IoT Mobile Edge Computing Networks Using a DF/AF UAV-Enabled Relay with Downlink NOMA. In: ISIEA (2023).
11. F. Vhora and J. Gandhi: A Comprehensive Survey on Mobile Edge Computing: Challenges, Tools, Applications. In: 4th ICCMC (2020).

12. A.-N. Nguyen, V.-N. Vo, C. So-In, and D.-B. Ha: System Performance Analysis for an Energy Harvesting IoT System Using a DF/AF UAV-Enabled Relay with Downlink NOMA under Nakagami-m Fading. In: Sensors, no. 1, pp. 285 (2021).
13. A.-N. Nguyen, D.-B. Ha, T.-V. Truong, V.-N. Vo, S. Sanguanpong, and C. So-In: Secrecy Performance Analysis and Optimization for UAV-Relay-Enabled WPT and Cooperative NOMA MEC in IoT Networks. In: IEEE Access, vol. 11, pp. 127800–127816 (2023).
14. A.-N. Nguyen, V. N. Vo, C. So-In, D.-B. Ha, and V.-T. Truong: Performance Analysis in UAV-enabled Relay with NOMA under Nakagami-m Fading Considering Adaptive Power Splitting. In: 18th JCSSE (2021).
15. T. Zhang, Y. Xu, J. Loo, D. Yang, and L. Xiao: Joint Computation and Communication Design for UAV-Assisted Mobile Edge Computing in IoT. In: IEEE Trans. on Indus., vol. 16, no. 8, pp. 5505–5516 (2020).
16. K. L. Judd: Quadrature Methods. In: University of Chicago's ICE (2012).